Indian Journal of Chemistry
Vol. 62, October 2023, pp. 1091-1102
DOI: 10.56042/ijc.v62i10.6189

Synthesis, spectroscopic characterizations, and comparison of experimental, and theoretical results of N-(3-chloro-2-methylphenyl)-2-(3,4-dichlorobenzylidene) thiosemicarbazone

Hakan Bülbül*[a], Şehriman Atalay[a] & Aliye Gediz Ertürk[b]

[a] Department of Physics, Faculty of Science and Arts, OndokuzMayıs University, 55200-Atakum-Samsun, Turkey

[b] Department of Chemistry, Faculty of Science and Arts, Ordu University, 52200 Ordu, Turkey

E-mail: hbulbul@omu.edu.tr

Received 4 February 2023; accepted (revised) 21 September 2023

N-(3-Chloro-2-methyl phenyl)-2-(3,4-dichlorobenzylidene)hydrazine-1-carbothioamide has been synthesized by the condensation of 3,4-dichlorobenzaldehyde with (3-chloro-2-methyl phenyl)-3-thiosemicarbazide. The structure of the novel synthesized thiosemicarbazone compound is well-characterized by FT-IR and NMR spectroscopic methods, and X-ray experiment. The geometry from X-ray experiment of the compound has been compared using the Hartree-Fock (HF) and density functional theory (DFT) methods with the 6-31+G(d) basis set. The obtained results show that the calculated results can well reproduce the structure of the compound. Mulliken charge, MEP, FMO, and Hirshfeld surface analysis have also been performed for the structure.

Keywords: Thiosemicarbazone, X-ray, DFT, Hartree-Fock, Spectroscopy, MEP, HOMO-LUMO, HSA

Thiosemicarbazones, which are derivatives of thiourea, contain a thiocarbonyl group instead of a carbonyl. Therefore, they constitute a family of compounds very similar to semicarbazones. Thiosemicarbazones are obtained by condensation of suitable aldehydes or ketones with the free amine end at position four of thiosemicarbazide or substituted thiosemicarbazide (Scheme 1). In recent years, thiosemicarbazone compounds are among the organic compounds with heteroatoms that have been studied with great interest due to their wide range of pharmacological properties. In the activity of thiosemicarbazone, it has been observed that the different substituents in the carbonyl compounds and thiosemicarbazide end that make up the structure are determinative[1]. In particular, the stable complexes they form with transition metals due to their metal-chelating abilities, compared to the free ligand forms; they act as pharmacophores exhibiting very different functionalities[2]. Compounds containing a thiosemicarbazone end in their structure have their biological potentials such as antimalarial[3], antiviral[4], antimicrobial[5], antidiabetic[6], anti-HIV[7], herbicidal[8], antitumor[9], anti-inflammatory[10], antitrypanosomal[11], antituberculose[12], insecticidal[13], and antifungal effects[14]. In addition to these, it has been stated that while they act as both reagent and catalyst in heterocyclic synthesis and photochemistry, they also play a role in different applications as anion recognition material[15].

This paper aims to elucidate the structure of the N-(3-chloro-2-methylphenyl)-2-(3,4-dichlorobenzylid ene)hydrazine-1-carbothioamide molecule containing thiosemicarbazone. The compound was characterized by LC/MS-TOF analysis, IR, ^{1}H, and APT-^{13}C- NMR spectroscopies. The crystal structure of the title compound was determined by the X-ray single-crystal diffraction method. Besides, the theoretical calculations of the structural geometry, frontier molecular orbital (FMO), molecular electrostatic potential (MEP), Hirsfeld surface analysis for the title compound were studied for the first time. For the theoretical calculations, DFT/B3LYP and HF methods were used with the 6-31+G(d) basis set. We

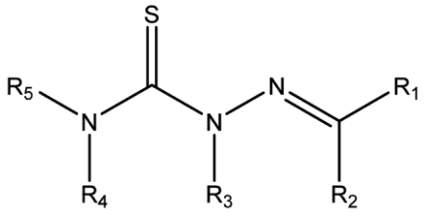

Scheme 1 — Thiosemicarbazone scaffold

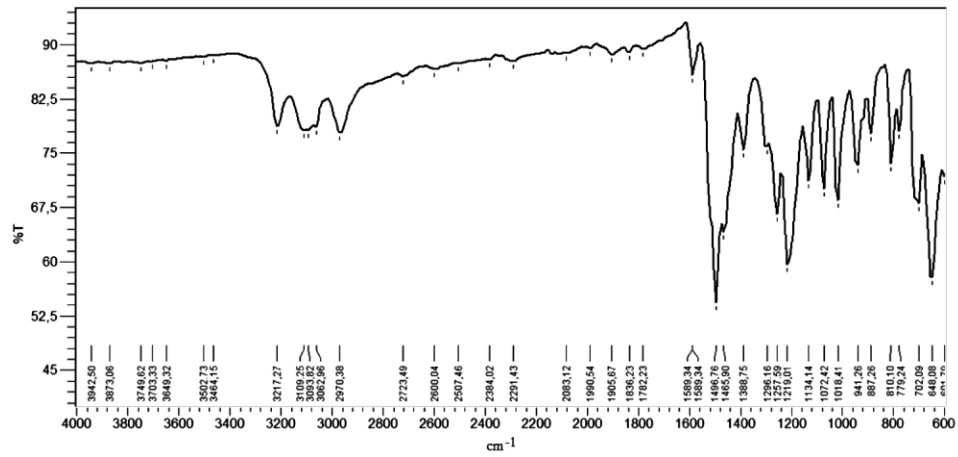

Fig. 1 — FT-IR spectrum of (**3**)

also made comparisons between experimental and theoretical structure.

Experimental Section

General Information

All chemicals were of reagent grade and used without any purification process. The uncorrected melting point of synthesized thiosemicarbazone was determined on a digital Electrothermal IA9200 instrument using Open capillaries. IR spectrum was performed on a Shimadzu IR Affinity-I FTIR-ATR spectrophotometer in the range of 4000 to 600 cm^{-1} at room temperature (Fig. 1). ^{1}H and APT-^{13}C signals in NMR spectra were recorded on a Bruker AVANCE III model 400 MHz spectrometer using deuterated DMSO as solvent at room temperature. The mass spectrum was performed on an Agilent LC/MS-TOF mass spectrometer. The progress of the reaction was monitored by TLC using UV detection using ethyl acetate: petroleum ether (2:3).

Synthesis of N-(3-chloro-2-methylphenyl)-2-(3,4-dichlorobenzylidene)hydrazine-1-carbothioamide (3)

In a round-bottom flask, 50 mg (0.232 mmol) of (3-chloro-2-methylphenyl)-3-thiosemicarbazide **(1)** was dissolved in 3 mL of ethanol. In another beaker, in to 41.82 mg (0.232 mmol) of 3,4-dichlorobenzaldehyde **(2)** dissolved in 3 mL of ethanol was added 2 drops of acetic acid (CH_3COOH). Following this the last mixture was dropped in to the first flask. It was boiled under reflux for 5 hours. The progress of the reaction was followed by thin layer chromatography in a 2:3 ethyl acetate:petroleum ether solvent system. After 5 hours, the reaction was terminated when the spot of the thiosemicarbazide compound disappeared. After the reaction mixture was evaporated, the solids recovered were washed with ethanol and diethyl ether and dried. The desired product **(3)** was then crystallized from acetonitrile by slow evaporation (12 days). Colorless solid, Yield: 73%; Rf: 0.45; m.p.: 227-228 °C. FTIR (ATR, υ, cm−1): 3217, 3109 (υ NH thiosemicarbazone), 2970 (aliph υ CH), 1589 (υ C=N), 1497 and 1465 (υ C=C benzene ring), 1388 (υ N-C=S), 1219 (υ C-N bending), 1018 (υ N-N), 810 (υ C= S), 702 (υ C-Cl); ^{1}H NMR (400 MHz, DMSO-d6, δ, ppm) 12.06 (s, ^{1}H, NH), 10.26 (s, ^{1}H, NH), 8.37 (s, ^{1}H, N=CH), 8.11 (s, ^{1}H, dichlorophenyl =CH), 7.80 (d, J: 8.4 Hz, ^{1}H dichlorophenyl =CH), 7.68 (d, J: 8.4 Hz, ^{1}H dichlorophenyl =CH), 7.43 (d, J: 7.7 Hz, ^{1}H, 3-chloro-2-methylphenyl =CH), 7.28 (t, J: 7.8 Hz, ^{1}H, 3-chloro-2-methylphenyl =CH), 7.24 (d, J: 7.4 Hz, ^{1}H, 3-chloro-2-methylphenyl = CH), 2.24 (s, 3H, -CH3); APT-^{13}C NMR (100 MHz, DMSO-d6, δ, ppm) 177.77, 140.50, 140.24, 135.44, 134.82, 134.00, 132.51, 132.28, 131.26, 128.89, 128.69, 128.68, 128.17, 127.31, 15.75; LC/MS-TOF: calculated for C15H12Cl3N3S (M + H)+ = 371.9890, found (M + H)+ = 371.9855.

X-ray crystallographic study

Detailed information about data collection, analysis, and refinement for **(3)** are given in Table 1. Intensity data were collected on a Bruker D8 QUEST diffractometer at 293(2)K using monochromate MoK_α radiation (λ=0.71073Å, graphite crystal monochromator). The molecular structure was defined using SHELXS97[16] and direct methods; and refined on F^2 by full-matrix least-squares with anisotropic thermal parameters for all atoms, except hydrogen atoms using SHELXL2014[17].

The hydrogen atoms were placed at calculated positions geometrically, with the C-H distances of 0.93-0.96Å, and refined using the riding model, with $U_{iso}(H)=1.2U_{eq}(C)$ and others (ethyl and methyl) $1.5U_{eq}(C)$.The reason for the slightly higher R and wR2 values may be the poor quality of the crystal, small crystal sizes and crystal defects.

Results and Discussion

Spectral analysis

The substituted thiosemicarbazide**(1)** reacted with 3,4-dichlorobenzaldehyde **(2)** in refluxing abs EtOH in the presence of a catalyst to afford the respective thiosemicarbazone **(3)** (Scheme 2). The characterization of the compound was performed by the data from FTIR, NMR (^{1}H and ^{13}C), and LC/MS-TOF spectroscopies. IR spectrum analysis indicated the basic peaks of absorption overlap exactly with the functional groups in the target compound. According to Fig. 2, the stretching peaks at 3217 and 3109 cm^{-1} are attributed to the NH group, while the bands at 1589 and 810 cm^{-1} are assigned to C=N (imine) and C=S groups, respectively[20]. In addition to other bands, the aromatic ring (C=C) was found the absorptions at 1497 and 1465 cm^{-1}. The band referring to the C-Cl group was seen at 702 cm^{-1}. Comparative experimental and theoretical IR values are given in Table 2. The values observed in the characteristic bands of (**3**) are close to the values of similar structures reported in the literature[21,22].

In the ^{1}H NMR spectrum (Fig. 3), we clarify the singlet peaks at 12.06, 10.26, and 8.37 ppm which are assigned to two NH groups bonded to the thiocarbonyl and imine (HC=N) group, respectively[23]. The peaks for the aromatic rings in the thiosemicarbazone **(3)** compound are given as follows: The peaks of the chlorinated aromatic ring from the aldehyde **(2)** are one singlet at 8.11 and two doublet peaks with J values of 8.4 Hz at 7.80 and 7.68, the aromatic ring peaks from the thiosemicarbazide (**1**) are at 7.43 and 7.24 ppm two doublets and a triplet signal at 7.28 ppm[24]. Finally, the singlet for three protons at 2.24 ppm belongs to the methyl group attached to the aromatic ring of thiosemicarbazide.

The formation of the targeted compound was also evaluated with the data of the ^{13}C spectrum (Fig. 4). The signal at 177.77 ppm was attributed to the thiocarbonyl (C=S) group[25]. In the area of 140.24 to 127.31 ppm, the aromatic rings signals are observed[26]. In addition, the signal at 15.75 ppm belongs to the methyl group bound to the aromatic ring of the thiosemicarbazide part.

Data conforming to the structural characterization of thiosemicarbazone **(3)** was also obtained from the mass spectrum. Our compound could be identified by the [M+H] peak[27]. The calculated [M+H] value of the formula $C_{15}H_{12}Cl_3N_3S$ is 371.9890, while this value

Table 1 — Crystallographic data for (3)

Chemical formula	$C_{15}H_{12}Cl_3N_3S$
Formula weight	372.69
Crystal system	Monoclinic
Crystal shape/color	Prism/Colorless
Temperature (K)	293(2)
Space group, Z	*C2/c*, 8
a, *b*, *c* (Å)	13.9595 (11), 8.1453 (11), 29.133 (3)
β (°)	95.797 (5)°
V (A^3)	3295.6 (6) $Å^3$
D_x(Mg cm^{-3})	1.502 g cm^{-3}
Radiation type	MoKα
μ (mm^{-1})	0.68 mm^{-1}
F_{000}	1520
Crystal size (mm^3)	0.040 × 0.020 × 0.015 mm
Data collection	
Diffractometer/meas.meth	Bruker D8 QUEST/φ and w-scans
Number of measured, independent, and observedreflections	45339, 2925, 2498
Criterion for observed reflections	$I > 2\sigma(I)$
R_{int}	0.092
θ_{max}	25.0°
Refinement	
Refinement on	F^2
$R[F^2>2\sigma(F^2)]$, wR, S	0.126, 0.319, 1.16
Number of reflections	2925
Number of parameters	200
$\Delta\rho_{max}$, $\Delta\rho_{min}$ ($eÅ^{-3}$)	1.54, −0.85 e / $Å^3$
Programs	Wingx, PLATON [18, 19]
CCDC	2162008

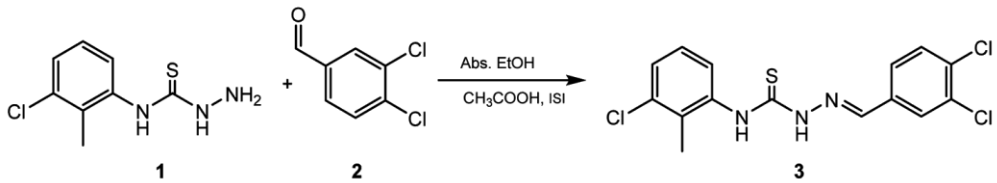

Scheme 2 — Chemical diagram of the title structure

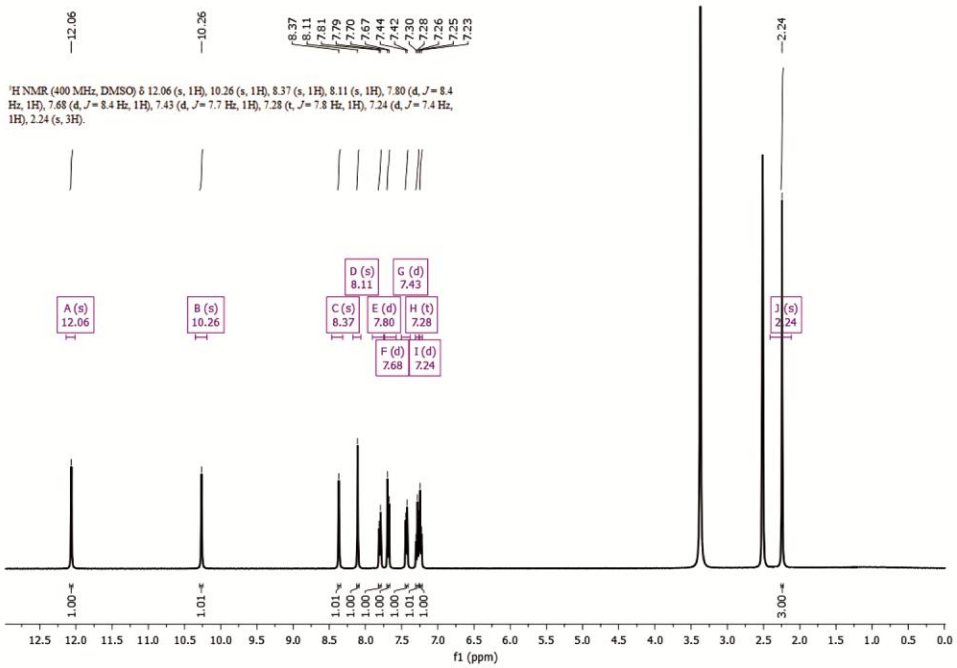

Fig. 2 — ^{1}H NMR spectrum of (**3**) in DMSO-d_6

Table 2 — Some selected experimental and theoretical vibrational bands of (3)(cm^{-1})

Vibrations	Experimental	DFT	HF
ν (N-H) thiosemicarbazone	3217 - 3109	3265 - 3239	3225 - 3212
ν (C-H)	2970	2980-2821	2874- 2710
ν (C=N)	1589	1537	1599
ν (C=C) benzene ring	1497 - 1465	1512 - 1468	1506 - 1483
γ (N-H) thiosemicarbazone	1388	1431 - 1419	1469 - 1421
ν(N-C=S)	1296	1314	1312
ν (N-N)	1018	1046	1034
ν (C=S)	810	822	840
ν (C-Cl)	702	731	720

found to be 371.9855 in the mass spectrum in Fig. 5. Thus, the proposed structure for thiosemicarbazone **(3)** was also approved by FT-IR, NMR, and mass spectroscopy techniques.

X-ray analysis

Ortep diagram of (**3**) is given in Fig. 5. The packaging diagrams showing the intermolecular interactions of the structure and the binding configuration are shown in Fig. 6. Geometric parameters of hydrogen bonds, crystal parameters, and data collection and purification information are given in Table 1.

(**3**) is not planar because the dihedral angle between C2/C7 and C10/C15 aromatic rings was determined as 65.30° (Fig. 4). The (**3**) is crystallized in the C2/c space group and packaged diagram contains 8 molecules in the unit cell. The tautomer structure of (**3**) is of the thion-imine form and has been stabilized by N-H···S and C-H···S type intermolecular hydrogen bonds. Geometry details of hydrogen bonds are given in Table 3. While the bond lengths of C8-N1 [1.352(10) Å] and C8-N2 [1.334(10) Å] of the carbon atom attached to the sulfur atom show a single bond character and, for the S1=C8 bond, a length of 1.679(8)Å shows the double bond character of this bond.These bond lengths, support the adoption of the thion-imine form. These bond lengths are in agreement with similar bond lengths in the thion-imine form in the literature[28]. Selected bond lengths, bond angles, and twist angles are listed in Table 4.

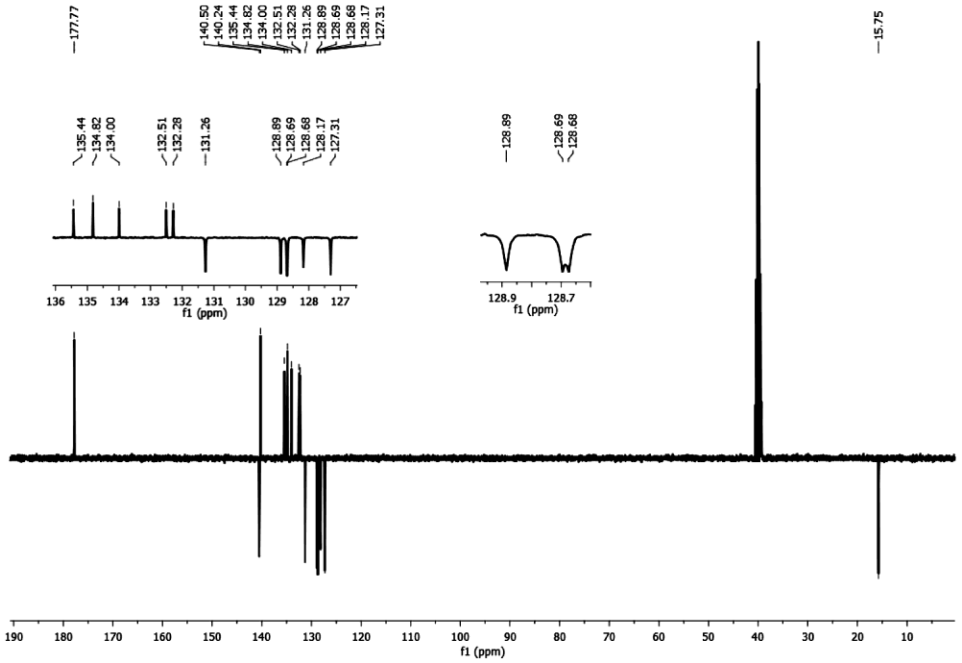

Fig. 3 — ^{13}C NMR spectrum of (**3**) in DMSO-d_6

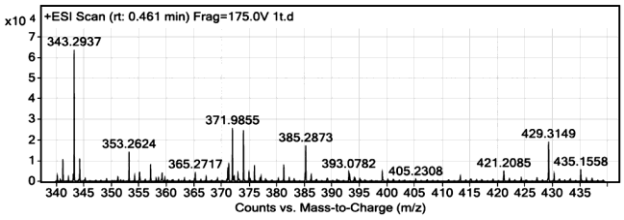

Fig. 4 — LC/MS-TOF spectrum of (**3**)

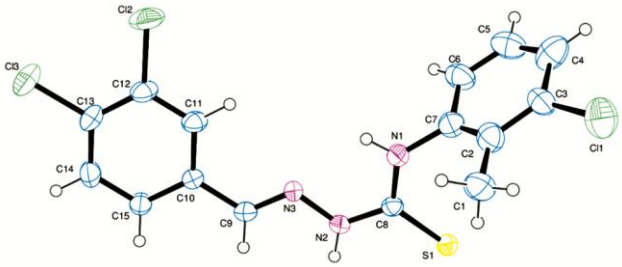

Fig. 5 — Ortep diagram of **(3)**

Computational studies

The DFT/B3LYP and HF methods were used for geometric optimization of (**3**). The 6-31+G(d) basis set was selected for the calculations. Gaussian 03[29] and Gaussview4.1[30]softwares were used for theoretical calculations. To make theoretical calculations in the Gaussian 03 program atomic parameter analyses of the molecule were used. The optimized geometric parameters of (**3**) were obtained and compared to each other. In addition, MEP and FMO analyses were calculated by using DFT/B3LYP method with the 6-31+G(d) basis set. Hirschfield surface analysis has been performed by the Crystal Explorer program[32].

Optimization geometry

HF and DFT methods are widely used in molecular modeling studies[33,34]. The minimum energy settlements of (**3**) were obtained by geometric optimization calculations using HF and DFT/B3LYP methods with 6-31+G(d) basis set. The minimum energy molecular settlement obtained as a result of the geometry optimization is given in Fig. 7. The bond length, bond angles, and torsion angles for (**3**) are given in Table 4.

The Root Mean Square Error (RMSE) values of the maximum difference and error squares mean for bond lengths and bond angles obtained from HF and B3LYP methods were examined in order to understand the accuracy of the calculated geometric parameters with the experimental data. For both bond lengths and bond angles, the B3LYP method appears to be more successful in representing experimental geometry.

When the figures and tables obtained from the computational methods were examined, the 5-position benzene ring in molecule pi-pi interaction with the benzene ring in position 4 caused the structure to bend (Table 4).

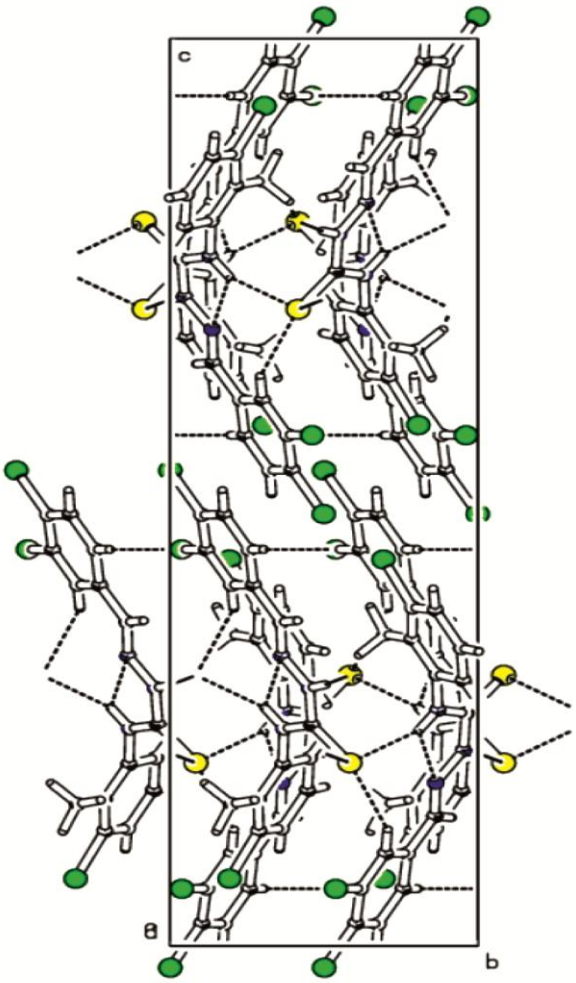

Fig. 6 — Package diagram of molecule **(3)**

Table 3 — Hydrogen bond geometry of (3)(Å)

D-H·*A*	*D*-H	H·*A*	*D*·*A*	*D*-H·*A*
N1-H1·S1^{i}	0.86	2.80	3.538 (8)	145
N2-H2·S1^{ii}	0.86	2.55	3.387 (7)	166
C11-H11·S1^{i}	0.93	2.86	3.731 (9)	156

(i)−x+1/2, y+1/2, −z+3/2; (ii) −x, y, −z+3/2

These RMSE values were obtained as 0.033Å and 2.47° for DFT and 0.030Å and 2.50° for HF for bond length and bond angles, respectively. It is seen that the RMSE value obtained by the HF method for bond lengths is smaller, and the RMSE value obtained by the DFT method for bond angles is smaller.

As a result, the HF method gave good results in calculating the bond lengths, while the DFT method gave better results in calculating the bond angles and the molecular geometry. Although there are some differences between experimental and theoretical studies, the DFT method will be quite sufficient in determining the physical and chemical properties of (**3**). The overlapping of the molecules was analyzed with the help of the CHEM3D program[35] for the experimental geometry comparisons with the geometries obtained as a result of the geometry optimizations (Fig. 8). Energy analysis was performed using the DFT method to understand whether the geometries obtained by geometry optimization were the minimum energy configurations and to investigate the minimum energy configuration of (**3**). For the energy analysis, the torsion angle T(C11-C10-C9-N3) of one of the aromatic rings was changed in 5° steps in the range of 0°/360° and the point energy was calculated one by one at each angle value (Fig. 7).

When the potential energy surface calculated in Fig. 8 is examined, two symmetrical potential barriers are observed at 90° and 270°. At these angle values, the rings are approximately perpendicular to each other and correspond to the highest energy configuration of the molecule. Three minima are observed on the potential energy surface around 10°, 195°, and 355°. The lowest energy one (global energy minimum) is around 10°, corresponding to the most stable configuration of the system. At this angle value, the total energy of the system was obtained as 0.1510 Hartree. It can be easily seen that from Table 4, both the X-ray and calculated values of the torsion angle T(C11-C10-C9-N3) correspond to the global energy minimum. This shows that the geometry obtained by geometry optimization has the lowest energy shaping.

HOMO-LUMO

The highest energy orbitals filled from the fundamental orbitals that constitute the mechanism of the reactions of the molecules; HOMO and the lowest vacant molecular orbitals are called LUMO. In chemical reactions, orbital energy, which tends to lose electrons, represents π-donor HOMO energy, and π-acceptor orbital energy, which tends to gain electrons, represents LUMO energy[30]. The HOMO and LUMO representations are obtained by the B3LYP method with the 6-31+G(d) basis set are given in Fig. 9.

The HOMO and LUMO values have energy values of −6.12 eV and −2.47 eV for (**3**), respectively. The energy difference between HOMO-LUMO orbitals was calculated as 3.65 eV. According to the results of the literature search for similar substances, the energy difference between HOMO-LUMO orbitals is near[36, 37].

Table 4 — Geometric parameters of (**3**)

Parameters	Experimental	DFT	HF
Bond lengths (Å)			
S1-C8	1.680 (8)	1.672	1.677
Cl3-C13	1.730 (9)	1.743	1.730
Cl2-C12	1.720 (9)	1.747	1.732
Cl1-C3	1.746 (12)	1.763	1.748
N3-C9	1.262 (11)	1.288	1.256
N3-N2	1.373 (9)	1.352	1.352
N1-C8	1.348 (11)	1.354	1.333
N1-C7	1.453 (13)	1.433	1.429
N2-C8	1.334 (10)	1.383	1.354
C10-C15	1.389 (12)	1.405	1.389
C10-C11	1.403 (12)	1.405	1.390
C10-C9	1.472 (12)	1.462	1.474
C11-C12	1.372 (13)	1.391	1.381
C12-C13	1.393 (14)	1.406	1.392
C15-C14	1.379 (13)	1.391	1.383
C13-C14	1.373 (14)	1.397	1.384
C7-C2	1.337 (15)	1.409	1.395
C7-C6	1.471 (16)	1.397	1.385
C6-C5	1.367 (17)	1.393	1.381
C3-C2	1.400 (14)	1.405	1.394
C3-C4	1.47 (2)	1.394	1.382
C2-C1	1.430 (15)	1.505	1.508
C4-C5	1.417 (19)	1.394	1.384
RMSE		0.033	0.030
Bond angles(°)			
Parameter	Experimental	DFT	HF
C9-N3-N2	117.0 (7)	118.0	117.9
C8-N1-C7	126.6 (8)	125.3	125.5
C8-N2-N3	121.1 (7)	122.5	122.5
C15-C10-C11	118.9 (8)	118.6	118.9
C15-C10-C9	120.2 (8)	119.1	119.1
C11-C10-C9	120.8 (8)	122.1	121.8
N3-C9-C10	121.2 (8)	122.5	122.4
N2-C8-N1	115.8 (7)	114.1	115.3
N2-C8-S1	120.2 (6)	119.2	118.9
N1-C8-S1	124.0 (6)	126.6	125.6
C12-C11-C10	119.6 (8)	120.7	120.6
C11-C12-C13	120.5 (8)	120.1	120.0
C11-C12-Cl2	118.9 (7)	118.6	118.3
C13-C12-Cl2	120.6 (7)	121.2	121.5
C14-C15-C10	121.1 (8)	120.7	120.5
C14-C13-C12	120.2 (8)	119.3	119.5
C14-C13-Cl3	119.0 (7)	119.0	118.6
C12-C13-Cl3	120.7 (7)	121.5	121.7
C2-C7-N1	122.5 (11)	120.4	120.3
C2-C7-C6	122.0 (10)	121.8	121.7
N1-C7-C6	115.5 (9)	117.6	117.7
C13-C14-C15	119.5 (8)	120.3	120.2
C5-C6-C7	116.8 (11)	120.1	120.2
C2-C3-C4	127.8 (12)	123.0	122.7
C2-C3-Cl1	119.3 (9)	119.4	119.7
C4-C3-Cl1	112.9 (9)	117.5	117.5
C7-C2-C3	116.7 (11)	116.0	116.3
C7-C2-C1	120.7 (11)	122.3	122.5
C3-C2-C1	122.5 (11)	121.5	121.1
C5-C4-C3	108.7 (15)	119.2	119.4
C6-C5-C4	127.8 (13)	119.6	119.4
RMSE		2.47	2.50
Torsion angles (°)			
Parameter	Experimental	DFT	HF
C9-N3-N2-C8	−179.1 (8)	178.4	179.5
N2-N3-C9-C10	−178.3 (8)	179.7	179.9
C15-C10-C9-N3	−174.6 (9)	178.9	−179.8
C11-C10-C9-N3	5.3 (14)	−1.05	0.1
N3-N2-C8-N1	3.9 (12)	1.7	1.01
N3-N2-C8-S1	−174.9 (6)	−178.4	−179.3
C7-N1-C8-N2	−175.4 (9)	−176.1	−178.1
C7-N1-C8-S1	3.2 (14)	4.1	2.2
C15-C10-C11-C12	−0.5 (14)	−0.08	−0.0006
C9-C10-C11-C12	179.6 (9)	179.9	−179.9
C10-C11-C12-C13	1.7 (15)	0.02	−0.002
C10-C11-C12-Cl2	−177.4 (7)	179.9	−179.9
C11-C10-C15-C14	0.6 (16)	0.08	0.0007
C9-C10-C15-C14	−179.5 (10)	−179.9	179.9
C11-C12-C13-C14	−2.9 (15)	0.03	0.004
Cl2-C12-C13-C14	176.2 (8)	−179.9	179.9
C11-C12-C13-Cl3	179.8 (8)	−179.9	−179.9
Cl2-C12-C13-Cl3	−1.1 (12)	0.04	−0.005
C8-N1-C7-C2	−77.1 (14)	−80.4	−91.2
C8-N1-C7-C6	105.0 (11)	102.1	91.2
C12-C13-C14-C15	2.9 (16)	−0.03	−0.004
Cl3-C13-C14-C15	−179.7 (9)	179.9	179.9
C10-C15-C14-C13	−1.8 (17)	−0.02	0.001
C2-C7-C6-C5	−0.8 (17)	0.2	0.09
N1-C7-C6-C5	177.2 (11)	177.6	177.6
N1-C7-C2-C3	−177.9 (9)	−178.3	−177.6
C6-C7-C2-C3	−0.1 (16)	−1.1	−0.1
N1-C7-C2-C1	0.4 (17)	1.7	2.9
C6-C7-C2-C1	178.2 (11)	179.0	−179.5
C4-C3-C2-C7	2.8 (17)	1.1	0.1
Cl1-C3-C2-C7	−177.2 (8)	−179.0	−179.7
C4-C3-C2-C1	−175.4 (11)	−179.0	179.5
Cl1-C3-C2-C1	4.6 (15)	0.7	−0.3
C2-C3-C4-C5	−4.1 (17)	−0.3	0.001
Cl1-C3-C4-C5	175.9 (9)	179.8	179.8
C7-C6-C5-C4	−1 (2)	0.5	0.01
C3-C4-C5-C6	3.1 (19)	−0.5	−0.06

(*contd.*)

Mulliken charge and molecular electrostatic potential map

The Mulliken charge analysis of (**3**) was obtained using the DFT and HF methods. When the Mulliken load distributions given in Table 5 are examined, differences can be seen according to the calculation methods chosen. Determining the charge distributions on each atom by separating a molecule into its atoms depends on the basis set used[38,39]. When the charge distributions of the molecule are examined, it is seen that the negative charges are concentrated on the electronegative sulfur, nitrogen, and carbon atoms. The S1 atom is in the appropriate position for the bond and has a negative charge. For this reason, it can be considered as the S1 atom's role as a proton acceptor in strong intermolecular hydrogen bonds. C11, N1, and N2 atoms have electro-positive charges. Since the C11 atom has a higher positive charge, it supports its role as a donor in the strong intermolecular C11-H11···S1 hydrogen bond. A molecular electrostatic potential (MEP) map was drawn in order to determine Mulliken charge distribution and molecular bonding regions and to see them in more detail (Fig. 10).

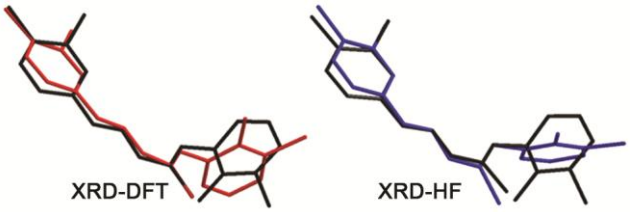

Fig. 7 — Overlaps of optimized geometries (XRD-black, HF blue and DFT red) of (**3**) obtained by experimental geometry and theoretical calculation methods.

The MEP surface shown in Fig. 10, superposition of electrostatic potential (attraction or repulsion of a positive charge for a molecule) is valuable for explaining the overall molecular charge distribution and also for predicting electrophilic addition sites. The red color represents negatively charged surface areas (*i.e*. areas where an electrophile is most favorable to accept). Another indicator of electrophilic attraction is provided by the local ionization potential energy surface, which is the superposition of electron removal (ionization) energy on electron density. The red-colored regions represent the regions on the molecular surface where electron removal is easiest (with minimal energy).

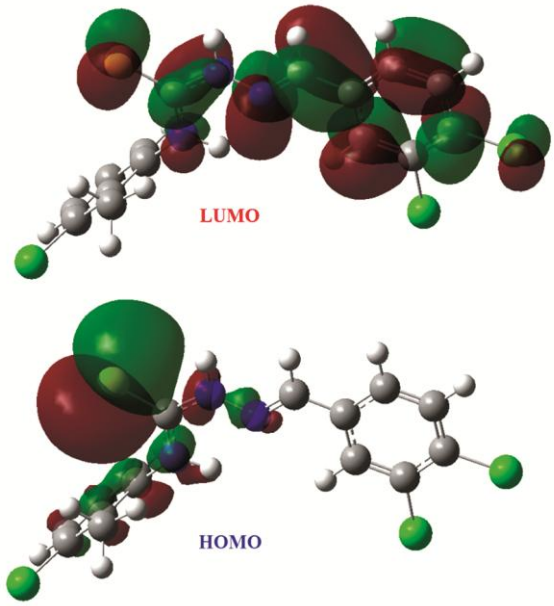

Fig. 9 — HOMO and LUMO configuration of **(3)**

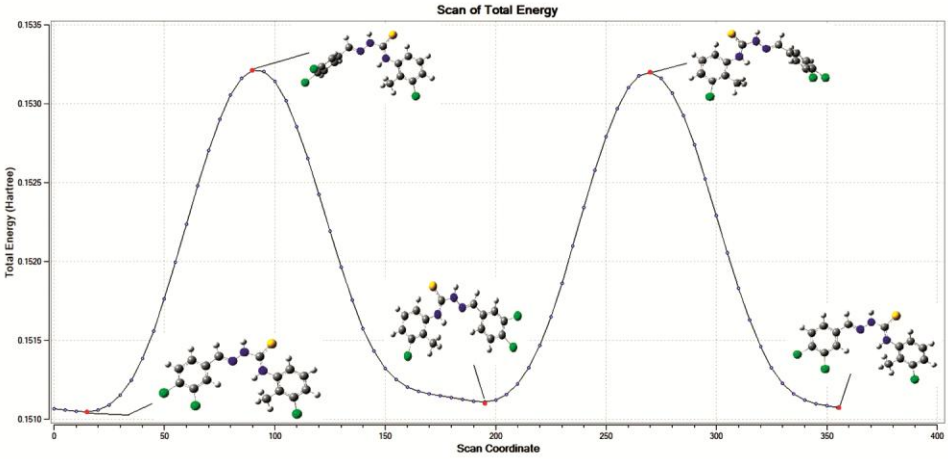

Fig. 8 — Energy change graph of (**3**) depending on torsion angle T(C11-C10-C9-N3)

Table 5 — Mulliken charge distribution of (3)(e)

Atom	DFT	HF
S1	−0.079266	−0.283155
Cl1	0.230054	0.250598
Cl2	0.260846	0.284265
Cl3	0.293043	0.326221
N1	−0.016679	0.006281
N2	0.024662	−0.022688
N3	0.154447	0.143558
C1	−0.320059	−0.297208
C2	−0.442418	1.150701
C3	0.648611	0.404486
C4	0.121720	−0.170368
C5	−0.072857	−0.158391
C6	0.779140	0.467104
C7	−0.821602	−1.576577
C8	−0.207767	0.032544
C9	−1.255451	−0.933007
C10	1.005173	0.685063
C11	0.939623	0.844001
C12	−0.446733	−0.266975
C13	−0.386518	−0.319189
C14	0.103819	0.053647
C15	−0.511787	−0.620910

The MEP calculations were obtained using the B3LYP/631+G(d) method. The MEP surface predicts the reactive sites of electrophilic or nucleophilic attack for the molecules. The negative (red and yellow) regions of MEP are related to nucleophilic activity and the positive (blue) regions are related to electrophilic activity as shown in Fig. 10.

When the MEP map is examined, the regions seen in red are on the sulfur atom. The maximum blue region is concentrated on hydrogen atoms bonded to nitrogen atoms. On the MEP map, the most negative region is on the S1 atom, and its value in atomic units is −0.027 a.u. The most positive region on the map was seen on the H atoms attached to the N1 atom in the substituents, and the MEP value was 0.057 a.u. According to these results, the S1 atom is the most suitable region in terms of electrophilic reaction in the structure.

Thermodynamic properties

On the basis of vibrational analysis and statistical thermodynamics, the standard thermodynamic functions: enthalpy (H^0_m), heat capacity ($C^0_{p,m}$) and entropy (S^0_m) were obtained at B3LYP/6-31+G(d) level and are listed in Table 6. As can be seen from the table, enthalpies, the heat capacities and entropies increase at any temperature from 100.00 to 500.00 K,

Table 6 — Thermodynamic properties

	Enthalpy H (J)	Heat Capacity C (J/K)	Entropy S (J/K.mol)
100	2.32	34.36	102.69
150	4.45	46.51	119.74
200	7.17	58.27	135.33
250	10.47	69.61	149.98
293	13.75	77.49	160.52
300	14.32	80.41	163.95
350	18.69	90.50	177.47
400	23.55	99.74	190.43
450	28.85	108.06	202.90
500	34.54	115.48	214.89

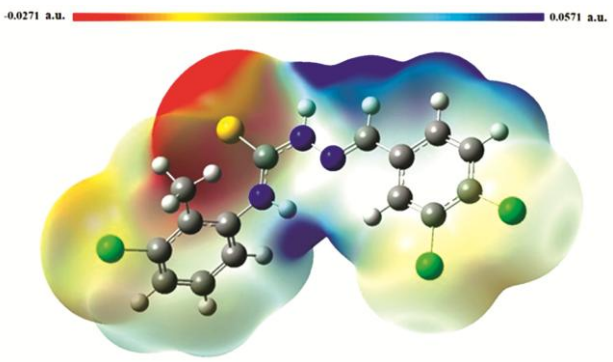

Fig. 10 — Calculated electrostatic potential surfaces on the molecular surfaces for (3).

because the intensities of molecular vibration increase with the increasing temperature[32].

The correlation equations between these thermodynamic properties and temperatures were fitted by quadratic formulas and the corresponding fitting factors are all beyond 0.999.

The correlation equations are as follows:

$$H^0_m = -0.72628 + 0.01932T + 1.02836 \times 10^{-4}T^2, (R^2 = 0.99994)$$

$$C^0_{p,m} = 7.34817 + 0.28058T - 1.27016 \times 10^{-4}T^2, (R^2 = 0.99955)$$

$$H^0_m = 69.43636 + 0.35019T + -1.19122 \times 10^{-4}T^2, (R^2 = 0.99969)$$

Hirshfeld Surface Analysis

The Hirshfeld surface analysis of (**3**)was carried out by the Crystal Explorer 21.5[32] program and the d_{norm}, d_e, and d_i Hirshfeld surfaces for the compound (Fig. 11) were created. These surfaces are 3D with d_{norm} −0.344 (red) and 1.326 a.u. Obtained in the (blue) color scale. Dark red dots on the Hirshfeld

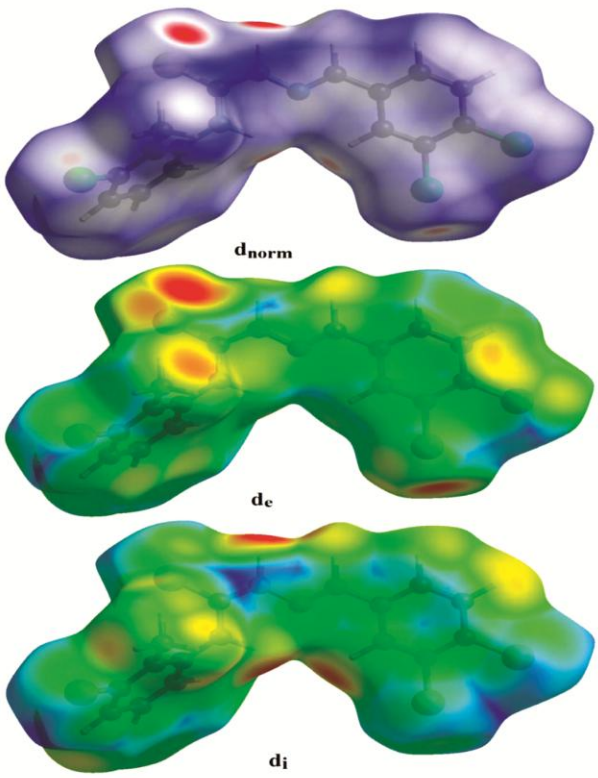

Fig. 11 — d_{norm}, d_e and d_i Hirshfeld surface of (**3**)

surface (d_{norm}) indicate stronger hydrogen bonds than light red dots. N1-H1···S1, N2-H2···S1, and C11-H11···S1 given in Table 3 confirm the hydrogen bonds. The regions seen in Fig. 12 show the rates of H····H, Cl···H, S···H, C···H, and N···H interactions. These ratios with the highest number of interactions in the structure were determined as 26.4%, 24.2%, 11.8%, 10.9%, and 4.1%, respectively. The representation of all interactions in the fingerprint region is given in Fig. 13. It was observed that the interactions of Hirshfeld surface analysis studies of similar structures were in regions near to **(3)**[40-42].

NLO

NLO effects arise from the interactions of electromagnetic fields in various media to produce new fields altered in phase, frequency, amplitude or other propagation characteristics from the incident fields[40]. NLO is at the forefront of current research due to its significance in providing the key functions of frequency shifting, optical logic, optical switching, optical modulation and optical memory for the emerging technologies in areas such as telecommunications, signal processing and optical interconnections[43].

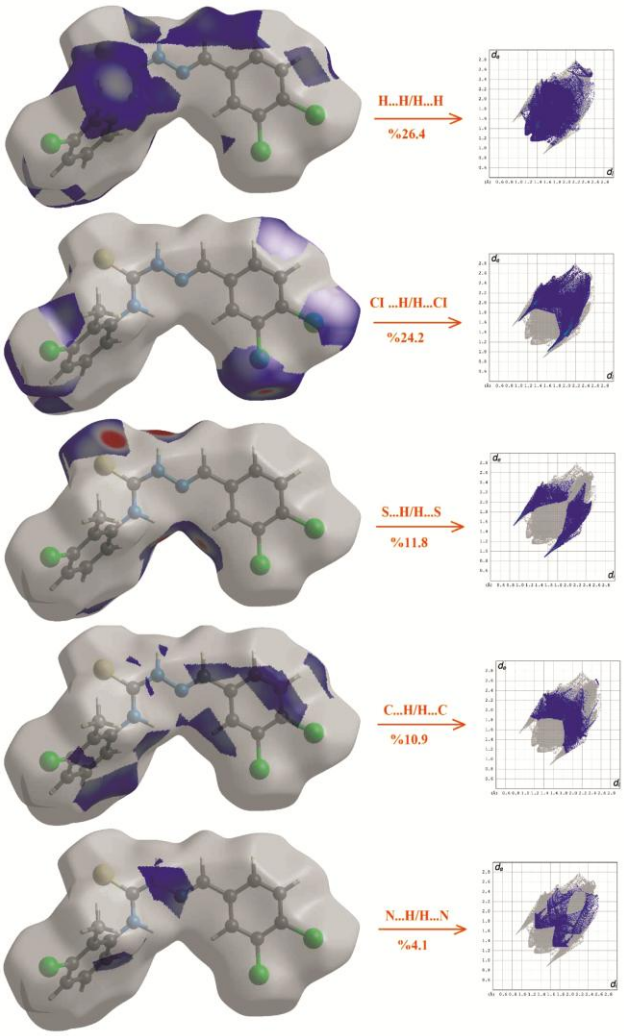

Fig. 12 — Interactions that contribute to the total Hirshfeld surface for (**3**)

DFT has been extensively used as an effective method to investigate the NLO materials[44]. The electronic dipole moment μ_i(i = x, y, z), polarizability α_{ij} and the first hyperpolarizability β_{ijk} of the title compound were calculated at the B3LYP/6-31+G(d) level using Gaussian 03W program package and listed in Table 7.

The calculated total dipole moment is equal to 3.9009 D. The calculated polarizability α_{tot}, is equal to 44.58205 Å^3. From Table 4, the calculated polarizability α_{ij} have nonzero values and was dominated by the diagonal components. The total first hyperpolarizability value β_{tot} of the title compound is equal to 14.1956 x 10^{-30} cm^5/esu which is greater than that of urea (the β_{tot} of urea is 0.77x10^{-30} cm^5/esu obtained by B3LYP/6-31+G(d) method). The first-order hyperpolarizability of the title compound is of

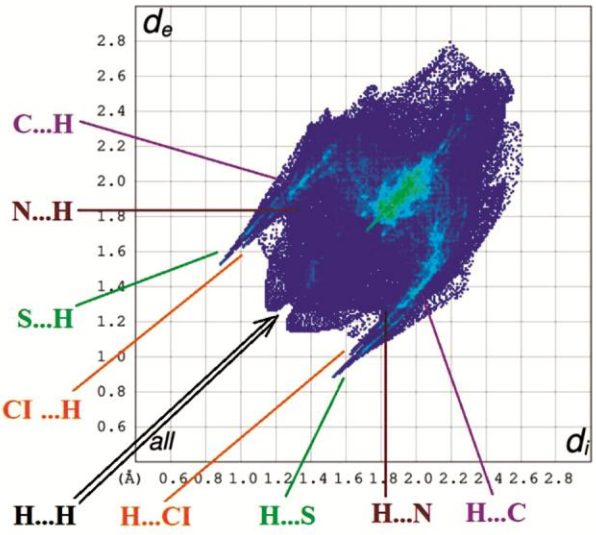

Fig. 13 — 2D finger print representation of (**3**)

Table 7 — The calculated dipole moment μ_{tot} (Debye), the average polarizability α_{tot} (Å^3) and- first hyperpolarizability β_{tot} (x10^{-30} cm^5/esu) for the title compound.

μ_x	−3.7727	β_{xxx}	−1481.2
μ_y	0.7106	β_{xxy}	−664.011
μ_z	0.6920	β_{xyy}	−151.365
μ_{tot}	3.9009	β_{yyy}	438.8403
α_{xx}	447.2571	β_{xxz}	40.6288
α_{xy}	15.15875	β_{xyz}	−55.1212
α_{yy}	266.5836	β_{yyz}	16.88126
α_{xz}	2.129872	β_{xzz}	8.896877
α_{yz}	−10.0095	β_{yzz}	71.49899
α_{zz}	188.6299	β_{zzz}	142.5088
α_{tot}	44.58205	β_{tot}	14.1956

18.43 times magnitude of urea, theoretically. The obtained results show that the title compound is a good candidate of NLO material[45].

Conclusions

The novel thiosemicarbazone derivative was synthesized by a one-pot acid-catalyzed condensation reaction and characterized using XRD, FTIR, NMR, and mass spectroscopic analysis methods. According to the XRD results, it was observed that the structure became stable in the monoclinic C2/c space group. The accuracy of the structure was confirmed according to the results of FTIR, NMR, and mass spectroscopy analysis. In addition, according to the theoretical calculations, it was seen that the HF method in calculating the bond lengths and the DFT method in the calculation of the bond angles gave better results, and it was determined that the theoretical calculation methods were close to the values obtained by the XRD method. It was observed that the packing diagram of the structure overlapped in the Mulliken charge analysis and MEP analysis performed with the DFT method. In the FMO calculation, it was calculated that the HOMO LUMO energy difference was 3.65 eV and it was decided that this difference was large enough and the structure was stable. Finally, the rates of bonding and interactions of the structure were determined by the Hirshfeld surface analysis.

The correlations between the thermodynamic properties H^o_m , $C^o_{p;\,m}$, S^o_m and temperatures T are also predicted. The predicted NLO properties of the title compound are much greater than those of urea. The title compound is a good candidate as a second-order nonlinear optical material[32]. The thiosemicarbazone compounds show pharmacological properties, the synthesized compound may be useful in pharmacological studies.We hope our paper will be helpful for the design and synthesis of new materials.

References

1 Pelosi G, *Open Crystallogr J*, 3 (2010) 16.
2 Lakovidou Z, Papageorgiou A, Demertzis M A, Mioglou E, Mourelatos D, Kotsis A, Yadav P N &Kovala-Demertzi D, *Anticancer Drugs*, 12 (2001) 65.
3 Klayman D L, Scovill J P, Bartosevich J F & Mason C J, *J Med Chem*, 22 (1979) 1367.
4 Padmanabhan P, Khaleefathullah S, Kaveri K, Palani G, Ramanathan G, Thennarasu S & Sivagnanam U T, *J Med Virol*, 89 (2017) 546.
5 Nibila T A, Soufeena P P, Periyat P &Aravindakshan K K, *J Mol Struct*, 1231 (2021) 1.
6 Shehzad M T, Hameed A, Al-Rashida M, Imran A, Uroos M, Asari A, Mohamad H, Islam M, Iftikhar S, Shafiq Z & Iqbal J, *Bioorg Chem*, 92 (2019)1.
7 Mishra V, Pandeya S N, Pannecouque C, Witvrouw M & Clercq E D, Arch Pharm Pharm Med Chem, 5 (2002) 183.
8 Xue S , Duan L, Ke S & Jia L, *Chem J Int*, 5 (2003) 67.
9 Guo C, Wang L, Li X, Wang S, Yu X, Xu K, Zhao Y, Luo J, Li X & Jiang B, *J Med Chem*, 62 (2019) 3051.
10 Bharti N, Athar F, Maurya M R & Azam A, *Bioorg Med Chem*, 12 (2004) 4679.
11 Casero R A, Klayman D L, Childs G E, Scovill J P & Desjardins R E, *Antimicrob Agents Chemother*, 18 (1980) 317.
12 Velezheva V, Brennan P, Ivanov P, Kornienko A, Lyubimov S, Kazarian K, Nikonenko B, Majorov K & Apt A, *Bioorg Med Chem Lett*, 26 (2015) 978.
13 Cheng W, Xiao T, Qian W, Lu T, Zhang T & Tang Xi, *Nat Prod Res*, 35 (2021) 3801.
14 Siwek A, Stefańska J, Dzitko K, Ruszczak A, *J Mol Model*, 18 (2012) 4159.
15 Guo Z, Wei C, Wang S, Qi F, He Z, Majeed U, Huang J, *J Mol Struct*, 1247 (2022) 1.

16 G M Sheldrick, *Acta CrystA*, 64 (2008) 112.
17 G M Sheldrick, *Acta CrystC*, 71 (2015) 3.
18 L J Farrugia, *J Appl Crystallogr*, 45 (2012) 849
19 Spek A L, *Acta CrystD*, 65 (2009) 148.
20 Govender H, Mocktar C, Kumalo H M &Koorbanally N A, *Phosphorus Sulfur Silicon Relat Elem*, 194 (2019) 1074.
21 Türkkan E, Sayin U, Erbilen N, Pehlivanoglu S, Erdogan G, Tasdemir H U &Akgemci E G, *J Organomet Chem*, 831 (2017) 23.
22 Kılıç-Cıkla I, Güveli Ş, Yavuz M, Bal-Demirci T, &Ülküseven B, *Polyhedron*, 105 (2016) 104.
23 Li J Q, Sun L Y, Jiang Z, Chen C, Gao H, Chigan J Z, Ding H H& Yang K W, *Bioorg Chem*, 107 (2021) 1.
24 Islam M, Khan A, Shehzad M T, Khiat M, Halim S A, Hameed A, Shah S R, Basri R, Anwar M U, Hussain J, Csuk R, Al-Harrasi A & Shafiq Z, *Bioorg Chem*, 109 (2021) 1.
25 Ezzat A, Mohamed M B I, Mahmoud A M, Farag R S, El-Tabl A S & Ragab A,*J Mol Struct*, 1251 (2022) 1.
26 Arooj M, Zahra M, Islam M, Ahmed N, Waseem A & Shafiq Z, *Spectrochim Acta A Mol BiomolSpectrosc*, 261 (2021) 1.
27 Toan V N, Thanh N D, Tri N M, Huong N T T, *Bioorg Med Chem Lett*, 30 (2020) 1.
28 Pasha A R, Khalid M, Shafiq Z, Khan M U, Naseer M M, Tahir M N & Jawaria R, *J Mol Struc*, 1230 (2021) 129852.
29 Frisch M J, Trucks G W, Schlegel H B, *Gaussian 03, Revision E 01*, (Gaussian, Wallingford, Conn, USA) 2004.
30 Dennington R, Keith T & Millam J, *GaussView, Version 4.1, Semichem*, (Shawnee Mission, Kan, USA) 2007.
31 Tanak H, J Phys Chem A, 115 (2011) 13865e.
32 Spackman P R, Turner M J, McKinnon J J, Wolff S K, Grimwood D J, Jayatilaka D, Spackman M A, *J Appl Crystallogr*, 54 (2021) 1006.
33 Khan S A, Adhikari A, Ayub K, Farooq A, Mahar S, Qureshi M N & Mahmood T, Spectrochim Acta Part A Mol Biomol Spec, 217 (2019) 113.
34 Tanak H, Koysal Y, Isik S, Yaman H & Ahsen V, Bull Korean Chem Society, 32 (2011) 673.
35 Chem Office protocol 2017. Available from: http://www.cambridgesoft.com/Ensemble_for_Chemistry/details/Default.aspx?fid=16andpid=735.
36 Balakrishnan N, Haribabu J, Malekshah R E, Swaminathan S, Balachandran C, Bhuvanesh N & Karvembu R, *Inorg Chimica Acta*, (2022) 120805. (https://doi.org/10.1016/j.ica.2022.120805).
37 Singh R K & Singh A K, *J Mol Str*, 1094 (2015) 61.
38 Mulliken R S, *J Chem Phys*, 23 (1955) 1833.
39 Lewars E, (2003) Density functional calculations. Computational Chemistry: Introduction to the Theory and Applications of Molecular and Quantum Mechanics, 385-445. (DOI: 10.1007/0-306-48391-2_7).
40 Yüksel B Ş, *J Mol Str*, 1229 (2021) 129617.
41 Pasha A R, Khalid M, Shafiq Z, Khan M U, Naseer M M, Tahir M N & Jawaria R. *J Mol Str*, 1230 (2021) 129852.
42 Al-Karawi A J M, OmarAli A A B, Dege N &Kansız S, *Chemical Papers*, 75 (2021) 3901.
43 Tanak H, Köysal Y, Isık S, Yaman H & Ahsen V, *Bull Korean Chem Soc*, 32 (2011) 673.
44 Andraud C, Brotin T, Garcia C, Pelle F, Goldner P, Bigot B & Collet A, *J Am Chem Soc*, 116 (1994) 2094.
45 Tanak H, Pawlus K, Marchewka M K, Pietraszko A, *Spectrochim Acta Part A*,118 (2014) 82.